Theory-Guided Synthesis of a Metastable Lead-Free Piezoelectric Polymorph

Lauren M. Garten,* Shyam Dwaraknath, Julian Walker, John S. Mangum, Paul F. Ndione, Yoonsang Park, Daniel A. Beaton, Venkatraman Gopalan, Brian P. Gorman, Laura T. Schelhas, Michael F. Toney, Susan Trolier-McKinstry, Kristin A. Persson, and David S. Ginley

Many technologically critical materials are metastable under ambient conditions, yet the understanding of how to rationally design and guide the synthesis of these materials is limited. This work presents an integrated approach that targets a metastable lead-free piezoelectric polymorph of $SrHfO_3$. First-principles calculations predict that the previous experimentally unrealized, metastable P4mm phase of $SrHfO_3$ should exhibit a direct piezoelectric response (d_{33}) of 36.9 pC N^{-1} (compared to $d_{33} = 0$ for the ground state). Combining computationally optimized substrate selection and synthesis conditions lead to the epitaxial stabilization of the polar P4mm phase of $SrHfO_3$ on $SrTiO_3$. The films are structurally consistent with the theory predictions. A ferroelectric-induced large signal effective converse piezoelectric response of 5.2 pm V^{-1} for a 35 nm film is observed, indicating the ability to predict and target multifunctionality. This illustrates a coupled theory-experimental approach to the discovery and realization of new multifunctional polymorphs.

Dr. L. M. Garten, Dr. P. F. Ndione, Dr. D. A. Beaton, Dr. D. S. Ginley
National Renewable Energy Laboratory
15013 Denver West Parkway, Golden, CO 80401, USA
E-mail: Lauren.garten@nrel.gov, lmg356@gmail.com
Dr. S. Dwaraknath, Prof. K. A. Persson
Lawrence Berkeley National Laboratory/University of California Berkeley
Berkeley, CA 94704, USA
Dr. J. Walker, Y. Park, Prof. V. Gopalan, Prof. S. Trolier-McKinstry
Department of Materials Science and Engineering and Materials
Research Institute
The Pennsylvania State University
University Park, PA 16802, USA
J. S. Mangum, Prof. B. P. Gorman
Colorado School of Mines
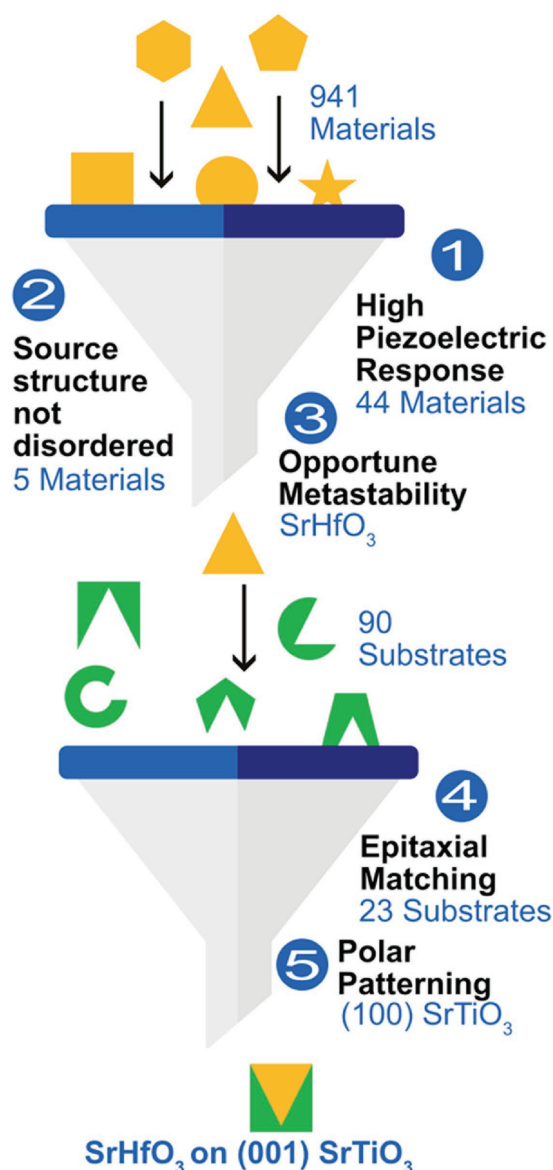Golden, CO 80401, USA
Dr. L. T. Schelhas, Dr. M. F. Toney
Applied Energy Programs
SLAC National Accelerator Laboratory
Menlo Park, CA 94025, USA
Dr. M. F. Toney
Stanford Synchrotron Radiation Lightsource
SLAC National Accelerator Laboratory
Menlo Park, CA 94025, USA
Prof. K. A. Persson
Department of Materials Science and Engineering
Hearst Mining Memorial Building, UC Berkeley
Berkeley, CA 94720, USA

The ORCID identification number(s) for the author(s) of this article can be found under https://doi.org/10.1002/adma.201800559.

Materials discovery drives many new technology-driven advancements, from consumer products, to renewable energy.[1,2] Recent advances in computational techniques[3] have significantly accelerated the prediction of promising multifunctional materials.[4] Multifunctional materials perform multiple functions in a system and can replace and outperform combinations of traditional materials, thus potentially reducing size, weight, cost, power consumption, and complexity while improving efficiency. In this work, a route to synthesize a theoretically predicted, metastable, multifunctional material using theory guidance is described and the predicted piezoelectric and ferroelectric functionalities definitively verified.

Here this approach is used to target high-response, lead-free piezoelectrics. Despite the technological importance of piezoelectrics, ranging from advanced medical instrumentation, to ultrasonic imaging systems, and compact actuators in industrial processes,[1] there are only a handful of piezoelectric materials that are routinely used. Because most commercially important piezoelectric ceramics are lead-based materials, one of the most popular being $Pb(Zr,Ti)O_3$, there has been a longstanding challenge to find lead-free piezoelectric materials.[5] Recently, Persson and co-workers[6] used density functional theory (DFT) to create a catalogue of piezoelectric tensors for 941 materials, and a large fraction are lead-free and metastable.[7]

Several materials in the Materials Project list exhibit promising intrinsic piezoelectric behavior, which can be quantified by comparing the maximum component of the piezoelectric tensor (e_{ij}^{max}). **Figure 1** illustrates the computational screening process that resulted in the identification of the $SrHfO_3$ as a possible novel, lead-free, high-performance piezoelectric. Over 900 piezoelectric materials were calculated, where 44 exhibit an e_{ij}^{max} greater than 3 C m^{-2} (the predicted piezoelectric e_{ij}^{max} for $PbTiO_3$). Upon inspection of the top 44, five materials emerged as potential candidates because they were not derived from previously known materials. A hitherto experimentally unrealized tetragonal P4mm polymorph of $SrHfO_3$[8] was deemed particularly promising due to its strong piezoelectric response of $e_{33} = 8.8$ C m^{-2}, and because nanofabrication routes exist for

Figure 1. Step-1 identifies the top-ranked highest piezoelectric materials in the Materials Project. Step-2 assesses the synthesizability of the material based on the origin of the compound. Step-3 identifies materials with low energy above hull. Step-4 then identifies effective substrates to stabilize the target materials. The final step, step-5 identified $SrTiO_3$ as the most promising substrate due to structure, availability, and surface polarization.

other polymorphs of this material, opening up a number of new opportunities for piezoelectric electronics development.[9] If stabilized, the P4*mm* phase should also exhibit ferroelectricity, which should add another extrinsic contribution to the piezoelectric response.[10]

Stabilizing a specific metastable polymorph can be challenging when a system presents strong polymorphism with small differences in metastability. The P4*mm* phase of $SrHfO_3$ is predicted to form 33 meV per atom above the ground state as defined by the convex hull, falling within the accessible range of synthesizable oxide polymorphs.[11] However, there

are four competing phases with energies less than the P4*mm*: the ground state P*nma* structure, another orthorhombic (C*mcm*), one tetragonal (I4/*mcm*) and one cubic (P*m$\overline{3}$m*).[12] Here, a previously developed combined lattice area and strain-matching algorithm[13] is employed to guide the substrate selection for epitaxial growth of the novel P4*mm* $SrHfO_3$ polymorph. Ideally the substrate would preferentially epitaxially stabilize the P4*mm* structure over other competing polymorphs. By examining the match between all possible $SrHfO_3$ polymorphs with a set of the 90 most common substrates, 23 possible substrate interfaces that could grow P4*mm* $SrHfO_3$ were identified. From these substrates, (001) cubic $SrTiO_3$ was chosen because it is a stable oxide that meets these epitaxial criteria and is commercially available.[14] A comparison of the strain energy and minimum lattice matching area for each $SrHfO_3$ polymorph enumerated above is shown in Table S1 (Supporting Information).

Pulsed laser deposition was used to grow epitaxial thin films from a $SrHfO_3$ target on $SrTiO_3$ single crystals substrates (and Nb-doped $SrTiO_3$ substrates for electrical measurements). The critical factors in the formation of highly oriented, phase pure P4*mm* $SrHfO_3$ by PLD are a temperature greater than or equal to 550 °C, a total pressure of 100 mTorrs oxygen, at a laser repetition pulse rate between 10 and 40 Hz and a thickness of 35 nm. Further processing details are provided in the Supporting Information. A transmission electron micrograph of the films is given in Figure S1 (Supporting Information). The focus of this study is on films that are ≈35 nm thick; films much thicker than this exhibited a second phase while films thinner than this were difficult to definitively characterize.

Phase formation was assessed by selected area electron diffraction (SAED), and reciprocal space mapping—X-ray diffraction (RSM-XRD). SAED down the [100] zone axis of a 35 nm thick $SrHfO_3$ thin film grown at 550 °C on a 0.7 wt% niobium-doped $SrTiO_3$ single crystal is shown in **Figure 2**a. The outer spots originate from the $SrTiO_3$ substrate, which has a cubic (P*m$\overline{3}$m*) structure. Interior to these reflections is an analogous set attributed to the epitaxial $SrHfO_3$ film due to its larger in-plane lattice parameters relative to $SrTiO_3$. Coincident alignment of the (001) and (011) reflections between the substrate and film indicate a fully epitaxial relationship and alignment of the *b* axes. Compressive in-plane stresses due to lattice matching of the $SrHfO_3$ film to the $SrTiO_3$ substrate can induce a Poisson effect, causing an expansion of the out-of-plane *c*-axis lattice parameter. The symmetry of the reflections in Figure 2a is consistent with this hypothesis and the P4*mm* structure, with $c{:}b = 1.002 \pm 0.0015$ and the *c*-axis of $SrHfO_3$ parallel to the growth direction. To further verify the P4*mm* structure against the other possible polymorphs, SAED was acquired down the [131] zone axis, shown in Figure S2 (Supporting Information). Using reflections from the [131] zone axis and measured *b* and *c* from the [100] zone axis, an $a{:}b = 1.000 \pm 0.0015$ was quantified. Furthermore, all additional reflections associated with other polymorphs of $SrHfO_3$ are absent, again confirming the presence of the P4*mm* tetragonal phase.

RSM-XRD and synchrotron X-ray diffraction further corroborates the structure determination by SAED. RSM-XRD of the (100), (113), and (224) planes was measured. A reciprocal space

ADVANCED
SCIENCE NEWS
www.advancedsciencenews.com

ADVANCED
MATERIALS
www.advmat.de
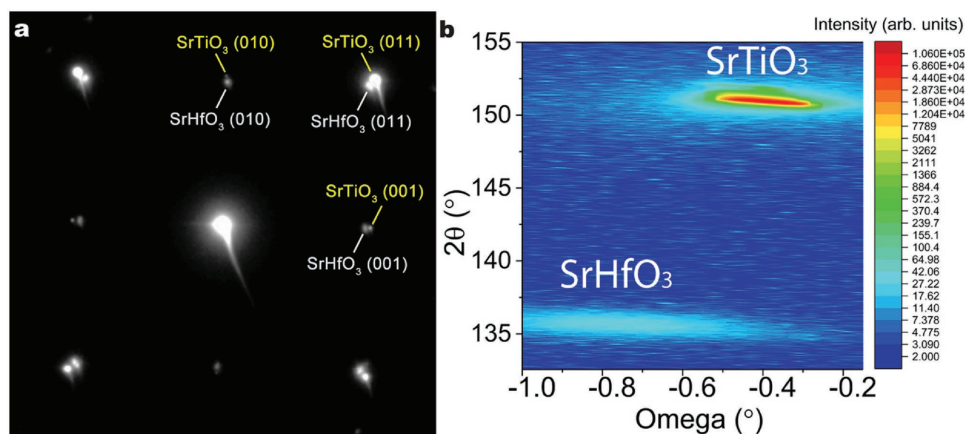
Figure 2. a) SAED of an $SrHfO_3$ thin film (white) on (001) $SrTiO_3$ single crystal substrate (yellow), looking down the [100] zone axis. b) RSM-XRD showing the (224) $SrHfO_3$ and $SrTiO_3$ peaks.

map for the (224) is shown in Figure 2b. The difference in the omega position for the substrate and $SrHfO_3$ film indicates that the film has partially relaxed. The structure determination is supported by 2D wide angle X-ray scattering, showing reflections consistent with those measured by RSM-XRD shown in Figure S3 (Supporting Information). The experimentally observed c:a lattice parameter ratio is identical with the Materials Project calculations, with c:a = 1.002 for the measured and predicted structure. The calculated lattice parameters from the RSM-XRD measurement are $a = b = 4.079 \pm 0.005$ Å and $c = 4.087 \pm 0.005$ Å, which is in close agreement with the SAED estimates.

Second harmonic generation (SHG) was used to definitively identify the presence of the polar $P4mm$ $SrHfO_3$ phase. SHG is often used to provide insight into the symmetry breaking in polar materials, as SHG is only seen in materials that lack a center of symmetry. Using optical SHG polarimetry analysis, the point group symmetry of the $SrHfO_3$ films was identified. Figure S4 (Supporting Information) shows the schematic drawing of transmission SHG polarimetry used in the study. **Figure 3**a shows SHG polar plot measurements taken at over a range of different angles; either fixed θ (−30° and +30°) or fixed ψ (0° and 90°), where angles θ is the incidence angle, and ψ is the sample rotation around the surface normal, as defined
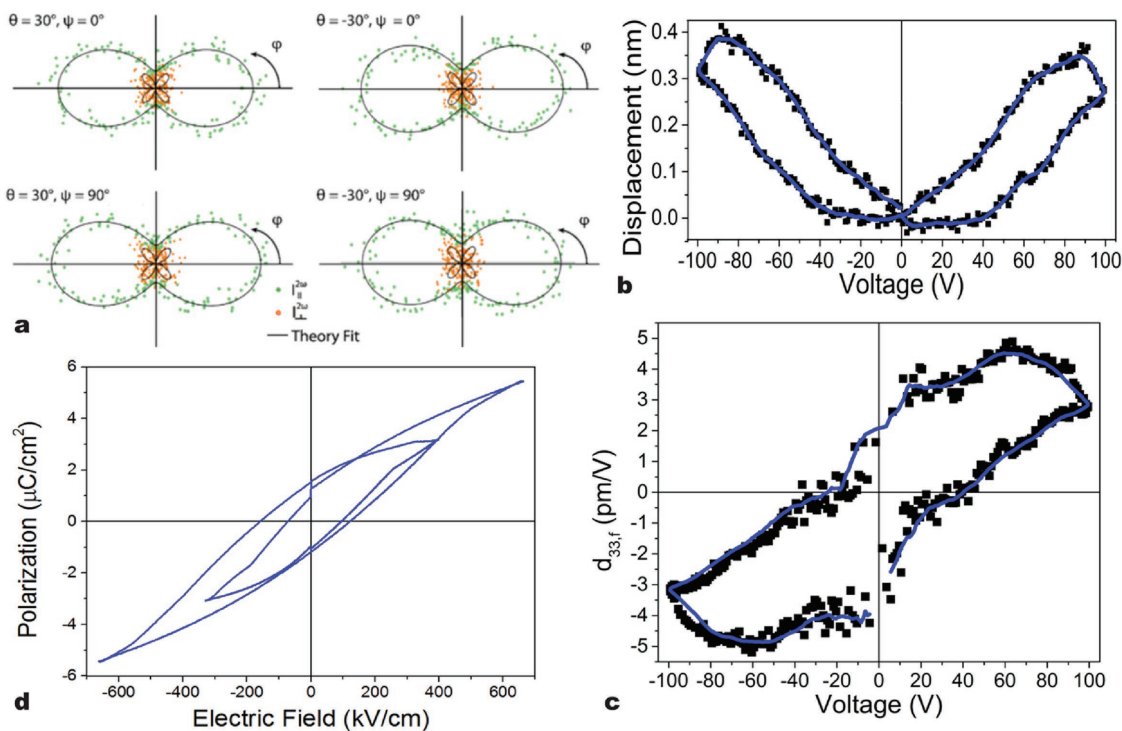
Figure 3. a) SHG intensity polar plots measured with fixed θ and ψ, showing a $4mm$ point group symmetry. b) The displacement measured as a function of voltage measured by double beam laser interferometry. c) The calculated effective d^*_{33} from the displacement in Figure 3a. d) The ferroelectric polarization-electric field loop.

Table 1. The DFT calculated d_{ij} piezoelectric tensor for $SrHfO_3$ [pC/N].

$$\begin{bmatrix} 0 & 0 & 0 & 0 & 58 & 0 \\ 0 & 0 & 0 & 58 & 0 & 0 \\ -7.4 & -7.4 & 36.9 & 0 & 0 & 0 \end{bmatrix}$$

in Figure S4 (Supporting Information). All of the SHG polar plots were fitted simultaneously, revealing that $SrHfO_3$ has $4mm$ point group symmetry, in agreement with the predicted $P4mm$ tetragonal polymorphic phase of $SrHfO_3$.

In order to fully demonstrate the integrated approach combining synthesizability and functionality, the electromechanical response of these $SrHfO_3$ films was assessed. The DFT predicted d_{ij} piezoelectric tensor is shown in **Table 1**, with the e_{ij} piezoelectric coefficients in Table S2 (Supporting Information). In order to vet the piezoelectric predictions, direct piezoelectric and dielectric measurements were made via a double beam laser interferometer. Initial small signal sweeps did not produce a significant piezoelectric response. However, after the application of an electric field of 220 kV cm^{-1} to reorient the polarization through the thickness of the films, a measurable displacement was observed. The measured piezoelectric displacement as a function of applied voltage for a single measurement (black), and the average of ten measurements (blue) is shown in Figure 3b. Hysteresis in the response as a function of the voltage history, and the offset in the forward and reversed sweep indicate that this is a ferroelectric-induced piezoelectric response and not solely due to electrostriction. The large signal effective $d*_{33,f}$ piezoelectric response, shown in Figure 3c, was calculated from these displacement measurements. The measurements show a maximum of 5.2 pm V^{-1}, which is in reasonable agreement with predictions of piezoelectricity in this material. For comparison, the d_{33} for other lead-free piezoelectrics AlN and GaN are 5.1 and 3.1 pm V^{-1}, respectively.[15] The fact that the measured response is lower than the predicted values is likely due to a combination of substrate clamping, in-plane strain and scaling effects in thin films,[16] as the piezoelectric response is known to decrease rapidly for films thinner than 100 nm.[17]

These $SrHfO_3$ films exhibit a ferroelectric enhanced piezoelectric response, further confirming the predictions of ferroelectricity in these materials.[10,18] Figure 3d shows the polarization-electric field (PE) response for a representative $SrHfO_3$ film. The average coercive field, and remnant polarization are 83 kV cm^{-1} and $\approx$1.2 μC cm^{-2} respectively. The pinching could be related to the rapid rate of deposition introducing defects in the film. Rayleigh analysis provides further support for the contribution of ferroelectric domain walls to the piezoelectric response in the $SrHfO_3$ films.[19] The Rayleigh response is the linear change in permittivity under an applied electric field, E_{AC}, due to the irreversible movement of ferroelectric domain walls, domain clusters, or phase boundaries.[20] The Rayleigh response as a function of temperature is shown in Figure S5 (Supporting Information). A positive Rayleigh response is observed for all temperatures measured between -20 °C and 50 °C. The Rayleigh response was fit to the minor PE-loops and found to be in good agreement. This indicates that the films have mobile boundaries that also contribute to the piezoelectric response.

The ability to rapidly identify and synthesize lead-free piezoelectric materials, as was achieved here, represents a step toward developing new multifunctional materials. Rapidly proposing and producing new functional materials will have an impact on a number of applications: medical transducers, energy harvesters and sensors, and electrical components.[1,21] The unique ability to integrate $SrHfO_3$ with silicon nanofabrication,[22] suggests that these materials would be good candidate material for dielectric energy storage or ferroelectric memory.

In conclusion, this work shows that metastable piezoelectric $P4mm$ phase of $SrHfO_3$ can be stabilized at room temperature. Beyond this, the methods that have been developed provide a theory-guided synthesis approach for the growth of metastable, DFT-predicted, lead-free, piezoelectric materials. The integration of an approach to synthesizability and functionality marks an advance in materials by design and should be applicable in a number of material systems.

Experimental Section

Theory: The first-principles results presented in this work was performed using the projector augmented wave method[23] as implemented in the Vienna Ab Initio Simulation Package.[24] In all calculations, the Perdew–Burke–Ernzerhof Generalized Gradient Approximation (GGA) for the exchange-correlation functional was employed.[25] The cut-off for the plane waves was 1000 eV and a uniform k-point density of $\approx$2000 per reciprocal atom (pra) was employed, which means that the number of atoms per cell multiplied by the number of k-points equals $\approx$2000. Similar to the previous work,[7] it was expected to correctly converge to ferromagnetic and nonmagnetic states in this way, but not to antiferromagnetic states. Due to the presence of strongly correlated electrons in some of the oxides, the GGA+U method was employed, with U representing the Hubbard-parameter.[26] The values of U were chosen consistent with those employed in MP.[6]

Thin Film Growth: Thin films of $SrHfO_3$ were deposited from a $SrHfO_3$ target (99.99% Materion) onto (100) oriented 0.7 wt% Nb-doped and undoped $SrTiO_3$ single crystal substrates (MTI Corp.) and platinum coated silicon (MTI Corp.) substrates by pulsed laser deposition. The pulsed laser deposition (PLD) system employed a 248 nm KrF laser, laser energy of 400 mJ and pulse frequencies of 40 Hz. The target substrate distance was 10 cm. Optimal films were deposited at temperatures from 500°C to 750 °C and pO$_2$ of 10^{-1} Torr.

Transmission Electron Microscopy (TEM): TEM micrographs were acquired with an FEI Co. Talos F200X transmission electron microscope operating at an accelerating voltage of 200 keV. Specimens for TEM were prepared from deposited films via in situ focused ion beam lift-out methods[27] using an FEI Co. Helios Nanolab 600i SEM/FIB DualBeam workstation. Specimens were ion milled at 2 keV and 77 pA to minimize Ga ion beam damage and achieve a final thickness of $\approx$80 nm. Structural characterization was conducted by acquiring SAED patterns on an FEI Co. Ceta 16M pixel CMOS camera at a camera length of 410 mm. The $SrTiO_3$ single crystal substrate was used to calibrate the camera constant, allowing SAED reflections to be accurately measured and indexed.

Reciprocal Space Mapping X-ray Diffraction: High-resolution X-ray diffraction of the films was performed on a Rigaku Smartlab X-ray diffractometer using a 2xGe(220) monochromator and a Hypix 2d detector operated in 1D mode. Reciprocal space maps used a 2xGe(220) analyzer crystal.

Second Harmonic Generation- Experimental Setting: Transmission SHG polarimetry measurements were performed in a far-field transmission configuration with 800 nm fundamental laser beam generated by Empower 45 Nd:YLF Pumped Solstice Ace Ti:Sapphire femtosecond laser system, with pulse width of 95 fs and repetition rate of 1 kHz.

**ADVANCED
SCIENCE NEWS**

www.advancedsciencenews.com

**ADVANCED
MATERIALS**

www.advmat.de

Piezoelectric, and Ferroelectric Measurements: Polarization-electric field hysteresis measurements were made with a Precision Multiferroic Precision Materials Analyzer (Radiant Technologies Inc., Albuquerque, NM) using a triangular wave form driving electric field signal and a frequency of 100 Hz. A maximum voltage of 100 V was applied. To reach the maximum voltage magnitude, hysteresis loop cycles were run consecutively with incrementally increasing electric field magnitude in 50 kV cm^{-1} intervals.

Piezoelectric coefficients ($d_{33,f}$) were measured using an axiACCT double beam laser interferometer system with a TF Analyzer 2000 for polarization and current measurement. The $d_{33,f}$ piezoelectric response was taken after poling at 220 kV cm^{-1} voltage for 15 min.

Supporting Information

Supporting Information is available from the Wiley Online Library or from the author.

Conflict of Interest

The authors declare no conflict of interest.

[1] P. Muralt, R. G. Polcawich, S. Trolier-McKinstry, *MRS Bull.* **2011**, *34*, 658.

[2] N. Setter, D. Damjanovic, L. Eng, G. Fox, S. Gevorgian, S. Hong, A. Kingon, H. Kohlstedt, N. Y. Park, G. B. Stephenson, I. Stolitchnov, A. K. Tagantsev, D. V. Taylor, T. Yamada, S. Streiffer, *J. Appl. Phys.* **2006**, *100*, 051606.

[3] a) S. Curtarolo, D. Morgan, K. Persson, J. Rodgers, G. Ceder, *Phys. Rev. Lett.* **2003**, *91*, 135503; b) A. Jain, G. Hautier, C. J. Moore, S. Ping Ong, C. C. Fischer, T. Mueller, K. A. Persson, G. Ceder, *Comput. Mater. Sci.* **2011**, *50*, 2295; c) D. Gunter, S. Cholia, A. Jain, M. Kocher, K. Persson, L. Ramakrishnan, S. P. Ong, G. Ceder, presetned at 2012 SC Companion: High Performance Computing, Networking Storage and Analysis, Salt Lake City, UT, November **2012**; d) A. Jain, K. A. Persson, G. Ceder, *APL Mater.* **2016**, *4*, 053102.

[4] A. Jain, Y. Shin, K. A. Persson, *Nat. Rev. Mater.* **2016**, *1*, 15004.

[5] Y. Saito, H. Takao, T. Tani, T. Nonoyama, K. Takatori, T. Homma, T. Nagaya, M. Nakamura, *Nature* **2004**, *432*, 84.

[6] A. Jain, S. P. Ong, G. Hautier, W. Chen, W. D. Richards, S. Dacek, S. Cholia, D. Gunter, D. Skinner, G. Ceder, K. A. Persson, *APL Mater.* **2013**, *1*, 011002.

[7] M. de Jong, W. Chen, H. Geerlings, M. Asta, K. A. Persson, *Sci. Data* **2015**, *2*, 150053.

[8] R. Vali, *Solid State Commun.* **2008**, *148*, 29.

[9] M. D. McDaniel, C. Hu, S. Lu, T. Q. Ngo, A. Posadas, A. Jiang, D. J. Smith, E. T. Yu, A. A. Demkov, J. G. Ekerdt, *J. Appl. Phys.* **2015**, *117*, 054101.

[10] M. G. Stachiotti, G. Fabricius, R. Alonso, C. O. Rodriguez, *Phys. Rev. B* **1998**, *58*, 8145.

[11] W. Sun, S. T. Dacek, S. P. Ong, G. Hautier, A. Jain, W. D. Richards, A. C. Gamst, K. A. Persson, G. Ceder, *Sci. Adv.* **2016**, *2*, e1600225.

[12] B. J. Kennedy, C. J. Howard, B. C. Chakoumakos, *Phys. Rev. B* **1999**, *60*, 2972.

[13] H. Ding, S. S. Dwaraknath, L. Garten, P. Ndione, D. Ginley, K. A. Persson, *ACS Appl. Mater. Interfaces* **2016**, *8*, 13086.

[14] K. M. Rabe, *Curr. Opin. Solid State Mater. Sci.* **2005**, *9*, 122.

[15] C. M. Lueng, H. L. W. Chan, C. Surya, C. L. Choy, *J. Appl. Phys.* **2000**, *88*, 5360.

[16] T. M. Shaw, S. Trolier-McKinstry, P. C. McIntyre, *Annu. Rev. Mater. Sci.* **2000**, *30*, 263.

[17] J. L. Zhao, H. X. Lu, J. R. Sun, B. G. Shen, *Phys. B: Condens. Matter* **2012**, *407*, 2258.

[18] K. S. Manoj, S. Gulab, K. Tae Hyun, K. Seiji, S. K. Ram, J. F. Scott, *Eur. Lett.* **2014**, *107*, 26004.

[19] P. Bintachitt, S. Jesse, D. Damjanovic, Y. Han, I. M. Reaney, S. Trolier-McKinstry, S. V. Kalinin, *Proc. Natl. Acad. Sci. USA* **2010**, *107*, 7219.

[20] L. M. Garten, M. Burch, A. S. Gupta, R. Haislmaier, V. Gopalan, E. C. Dickey, S. Trolier-McKinstry, *J. Am. Ceram. Soc.* **2016**, *99*, 1645.

[21] T. R. Shrout, S. J. Zhang, *J. Electroceram.* **2007**, *19*, 113.

[22] M. Sousa, C. Rossel, C. Marchiori, H. Siegwart, D. Caimi, J.-P. Locquet, D. J. Webb, R. Germann, J. Fompeyrine, K. Babich, J. W. Seo, C. Dieker, *J. Appl. Phys.* **2007**, *102*, 104103.

[23] a) P. E. Blöchl, *Phys. Rev. B* **1994**, *50*, 17953; b) G. Kresse, D. Joubert, *Phys. Rev. B* **1999**, *59*, 1758.

[24] a) G. Kresse, J. Hafner, *Phys. Rev. B* **1993**, *47*, 558; b) G. Kresse, J. Furthmüller, *Phys. Rev. B* **1996**, *54*, 11169.

[25] J. P. Perdew, K. Burke, M. Ernzerhof, *Phys. Rev. Lett.* **1996**, *77*, 3865.

[26] a) V. I. Anisimov, J. Zaanen, O. K. Andersen, *Phys. Rev. B* **1991**, *44*, 943; b) S. L. Dudarev, G. A. Botton, S. Y. Savrasov, C. J. Humphreys, A. P. Sutton, *Phys. Rev. B* **1998**, *57*, 1505.

[27] L. A. Giannuzzi, F. A. Stevie, *Micron* **1999**, *30*, 197.